10th HSTAM International Congress on Mechanics
Chania, Crete, Greece, 25 – 27 May, 2013

SIMULATION OF SAILS OF A YACHT USING A FLUID-STRUCTURE INTERACTION MODEL

E. Angelou[1], K. Spyrou[1]

[1]School of Naval Architecture and Marine Engineering
National Technical University of Athens
9 Iroon Polytechneiou, Zographos 15780, Athens, Greece
E-mail: angeloum@mail.ntua.gr

Keywords: Sailing Yacht, Lifting Surface Vortex Lattice, Shell Finite Elements.

Abstract. *A mathematical model for the simulation of the motions of sails on yachts has been built. Sails provide the aerodynamic forces used for propulsion; but being very thin, they have their shape adapted according to the locally developing pressures. Thus the flying shape of a sail in real sailing conditions differs from its design shape and it is basically unknown. In this model the fluid-structure interaction problem of the sails is handled by a low order Boundary Element Method for the aerodynamic part (Lifting Surface), coupled with a finite element method for the structural part (Shell Elements) and an iterative scheme that provide the converged flying shape of the sail and the sustained forces and moments. A future version of this model is intended for course stability analysis of a yacht in waves.*

1 INTRODUCTION

Sails are surfaces of very small thickness and while this allows a major simplification in the fluid modelling, it simultaneously induces a drawback. This insignificant thickness makes the sail to be a very flexible surface, subjected to deformations due to the pressure forces it sustains under wind flow. Calculating the flow around them then is not enough, as one should be able to account for the difference between the design shape of the sail and the flying shape it adopts. Moreover, it is important to know the effect this bears to the forces and moments on the sail. Excluding wind tunnel tests and real-time measurements at sea, a common computational approach is to combine a fluid solver for the flow field around the sail with a structural solver for the transition of the initial to the new shape.

Regarding the aforementioned simplification, the small thickness of the sail makes it ideal for being modelled with a potential flow method, such as the one using the Lifting Surface Theory (L.S.T.). This is a formulation for lifting flows that allows the effects of camber and thickness to be decoupled and it is usually applied through a numerical scheme based on the Vortex Lattice Method (V.L.M.). While the lifting surface bears minimal computational cost, it requires that the flow always remains attached to the surface, thus restraining L.S.T.'s applicability to a relatively small range of fluid inflow angles. To examine the behaviour of a sail in a wider operational range where drag effects become dominant, the use of viscous flows methods such as RANSE solvers is unavoidable. These provide great detail of the flow field but induce a considerable computational cost. This would be incompatible with the longer term objective of the current work which is, to perform dynamic stability analysis of a yacht's motion considering the coupled aero-hydrodynamic problem.

Once the pressure around the sails is known, their new shape can be derived using a Finite Element Method formulation. While using a simple approach to derive the new shell shape is acceptable, such as describing the sail surface by a single type of shell element, this is too subjected to some errors: sails, being made of woven panels joined together and reinforced with fibers, are hardly isotropic.

There is a wide range of available research on the area of "flying" sail analysis. Ranzenbach et al [1], combined a potential flow vortex lattice formulation integrated with a viscous boundary layer for attached flows, with a quadrilateral element FEM solver that included the capability of modelling wrinkling effects of the sails. Graf et al [2] implemented a FEM solver of triangular elements into a RANSE commercial package to calculate the flow around downwind sails. Schoop et al [3] introduced the quasi-continuous Vortex Lattice Method, where the discrete vortex forces were transformed to a continuous pressure field around the sail, while the FEM solver consisted of higher order quadrilateral elements. Vernengo et al [4] applied the Vortex Lattice Scheme in a formulation very similar to the modelling we use here, and along with Trimarchi [5] coupled it with a FEM code of triangular membranes reinforced with cable elements. Many other research contributions to the problem are available through the literature, handling either the combined case or a specific component in increased detail.

In need of a relatively fast method to be coupled with a hull analysis solver, the choice has been made to use the Lifting Surface Vortex Lattice Method and a FEM using triangular shell elements with joint membrane and bending parts.

2 GENERAL FORMULATION

The sails are considered in an initial equilibrium with zero camber (flat surfaces). Using the wind velocity and angle of attack the Lifting Surface Theory is used to calculate the pressure difference between the two sides of each sail surface. This pressure is then used to calculate nodal forces on the vertices of the triangles. These forces are subsequently used as input to the Shell FEM module to calculate the nodal displacements. The deformed surface is directed as input to the Lifting Surface module and the procedure commences following an iterative scheme until the calculated between successive steps aerodynamic forces have converged, as in the flow diagram of Figure 1.

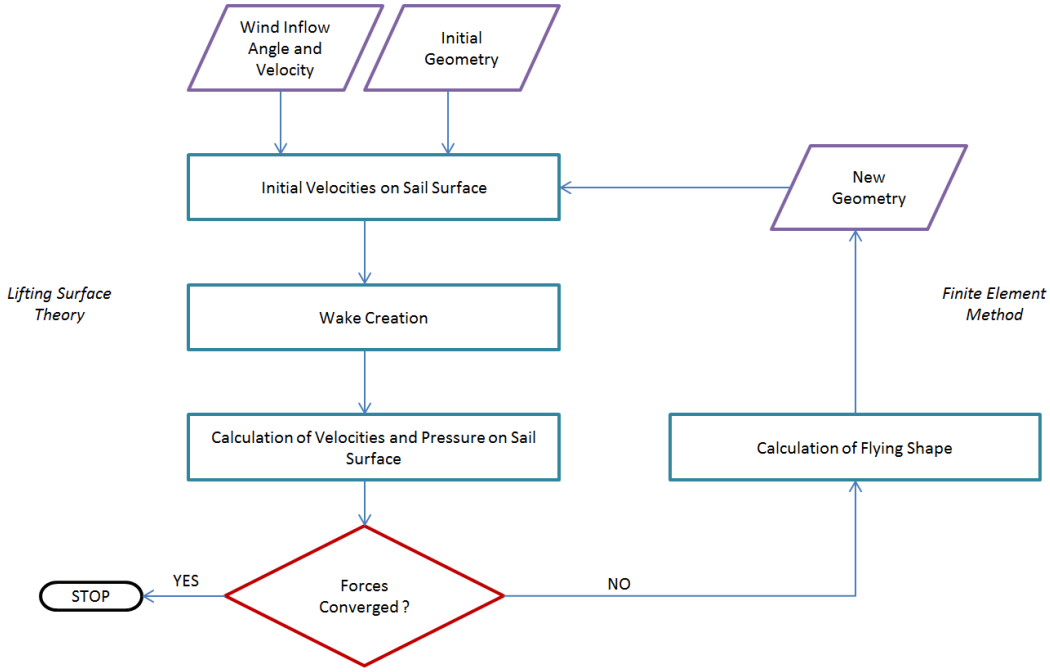

Figure 1. Algorithm Flow Diagram

2.1 Aerodynamic Part

Considering a body moving inside a large volume of inviscid, incompressible and irrotational fluid, then the fluid velocity can be described by the gradient of a scalar potential Φ which satisfies the Laplace Equation

$$\nabla^2\Phi = 0 \tag{1}$$

where $\Phi = \varphi + \Phi_\infty$, φ being the perturbation potential due to the presence of the body and Φ_∞ the free stream potential. In order to approach the system with a boundary value technique, we need to set a series of boundary conditions such as:

no entrance boundary condition $\quad \nabla\Phi \cdot \vec{n} = 0$ (2)

body induced disturbance decay far from the body $\quad lim_{r\to\infty} \nabla\Phi = \vec{V}_\infty$ (3)

where $\vec{V}_\infty$ is the free stream velocity and $\vec{n}$ the surface normal vector.

The L.S.T is actually a linearized Boundary Element Method offering a formulation that allows the effects of camber and thickness to be decoupled, and the no-entrance boundary condition to be transferred to the mean camber line of a surface. The Vortex Lattice Method is a numerical scheme that discretizes a surface into a series of rectangular panels, allowing so the real flow to be approximated by placing a series of discrete lines of vorticity instead of a continuous distribution along the field. It was introduced by Faulkner in 1943 [6] and since

then it has been used mainly for the study of single or multiple airfoils and extended over propellers and ship rudders.
In terms of the Lifting Surface Theory a system of constant strength horseshoe vortices is placed on every panel of the surface. The vortex induced velocity is evaluated using the Biot Savart Type Integral for the induced velocity of a vortex segment of constant strength **Γ** to any point **P**:

$$\overrightarrow{\boldsymbol{q}} = \frac{\boldsymbol{\Gamma}}{\boldsymbol{4\pi}} \int \frac{d\boldsymbol{l} \times (\vec{\boldsymbol{r}})}{|\vec{\boldsymbol{r}}|^3} \tag{4}$$

where $\vec{\boldsymbol{r}}$ is the vector from the segment $d\boldsymbol{l}$ to the point **P**. Derivation of equation (4) and the underlying theory is explained thoroughly on fluid dynamics literature as on Spurk [7]. Following the numerical treatment as in Katz et al [8], equation (4) transforms to the vectorial form :

$$\overrightarrow{\boldsymbol{q}} = \frac{\boldsymbol{\Gamma}}{\boldsymbol{4\pi}} \frac{\overrightarrow{\boldsymbol{r_1}} \times \overrightarrow{\boldsymbol{r_2}}}{|\overrightarrow{\boldsymbol{r_1}} \times \overrightarrow{\boldsymbol{r_2}}|} \overrightarrow{\boldsymbol{r_0}} \left(\frac{\overrightarrow{\boldsymbol{r_1}}}{\boldsymbol{r_1}} - \frac{\overrightarrow{\boldsymbol{r_2}}}{\boldsymbol{r_2}} \right) \tag{5}$$

where $\overrightarrow{\boldsymbol{r_0}}$ is the vector ($\overrightarrow{\mathrm{AB}}$), and $\overrightarrow{\boldsymbol{r_1}}, \overrightarrow{\boldsymbol{r_2}}$ are the position vectors of P from the filament's edges. The vortex consists of a parallel to the leading panel edge filament and two trailing filaments that run towards the trailing edge where the Kutta condition is satisfied and further to the wake. As the wake is a free shear layer, it can only carry vorticity. The flow being steady, it allows a first approximation for the free vortex sheet, with the vortex lines aligned with the initially undisturbed flow (frozen wake propagating aft on the direction of the free stream).

Each panel contains a control point **P** where the vortex induced velocity from the same or another panel is evaluated. The leading segment of every horseshoe vortex is placed on the ¼ each panel's chord line [8]. Root and tip trailing vortex segment are moved inwards by a quarter of an element span, as in Willis [9], for increased accuracy. The control point is placed on each panel on the ¾ of its chord line, where the boundary condition of no-entrance is to be satisfied. The induced velocity of every horseshoe vortex j to every point i can be represented by a matrix of influence coefficients A_{ij} and the no-entrance boundary condition reduces to a system of linear equations:

$$\sum_{i,j=1}^{N} A_{ij}\, \Gamma_j = -\vec{V}_\infty \cdot \vec{n} \tag{6}$$

Once the coefficient matrix has been calculated, the linear system is solved using LU decomposition for the strength of the horseshoe vortices. Solving of the circulation Γ allows for the calculation of the total velocities. Once these are known, the wake vortex lines are then rotated in order to apply the force free condition and to be aligned with the local total velocity vectors, providing so the roll-up of the wake until convergence is met, as in the steady case treatment of a 3D hydrofoil problem from Lee [10]. Finally the forces on the sail are calculated using the Kutta - Jukowski theorem for a vortex line of intensity $\vec{\Gamma}$ and tangential velocity $\vec{V}_t$:

$$\vec{\mathrm{L}} = \rho \cdot \vec{V}_t \times \vec{\Gamma} \tag{7}$$

2.2 Aeroelastic Part

We use the flat triangular shell element that consists of a membrane and a bending element. The membrane elements are Constant Strain Triangles (CST) while the bending elements are Discrete Kirchhoff Triangles (DKT). The flat elements are thus developed by superimposing the stiffness of the membrane and the bending elements.

The membrane contribution to the shell element is provided by the Constant Strain Triangle under plane stress conditions. As in Zienkiewicz [11a & 11b] we consider a single flat triangle element with three nodes and two degrees of freedom per node, totaling to six. Each node is allowed to move in the planar directions u and v (Figure 2a).

The shape functions for each node i, j, m are linear functions of x and y : $N_i = \frac{a_i + b_i x + c_i y}{2A}$ where: $a_i = x_y y_m - x_m y_j$, $b_i = y_j - y_m$, $c_i = x_m - x_j$ and A is the area of the triangle, while the rest of the coefficients are obtained by permutation of i, j, m. The membrane stiffness matrix for any triangular shell element {e} is [11a]:

$$K_{CSTe} = \int_A B_E^T D_E \; B_E \; \mathrm{t}\det[J]\, dx\, dy \tag{8}$$

where $B_E = \begin{bmatrix} \frac{\partial N_1}{\partial x} & 0 & \frac{\partial N_2}{\partial x} & & \frac{\partial N_3}{\partial x} & \\ & \frac{\partial N_1}{\partial y} & & \frac{\partial N_2}{\partial y} & & \frac{\partial N_3}{\partial y} \\ \frac{\partial N_1}{\partial y} & \frac{\partial N_1}{\partial x} & \frac{\partial N_2}{\partial y} & \frac{\partial N_2}{\partial x} & \frac{\partial N_3}{\partial y} & \frac{\partial N_3}{\partial x} \end{bmatrix}$ (9) is the strain displacement matrix and D_E is the elasticity matrix for plane stress. The product $B_E^T D_E \; B_E$ is free of *x* or *y* terms, so $K_{CSTe} = B_E^T D_E \, B_E \, t \, A$ (10).

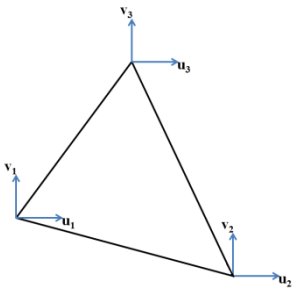

Figure 2a. Membrane Element (CST)

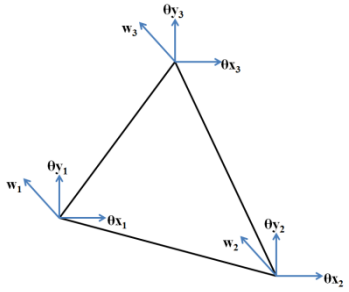

Figure 2b. Plate Element (DKT)

For the plate bending part we adapt the formulation of Batoz [12] and consider the Discrete Kirchhoff Triangle, an element with three nodes and three degrees of freedom per node, *w* being the normal to the triangle displacement and θ_x, θ_y the rotations around the x and y axis respectively (Figure 2b).

$$K_{DKTe} = 2A \int_{\eta=0}^{1} \int_{\xi=0}^{1-\eta} B_B^T \, D_B \; B_B \, d\xi \, d\eta \tag{11}$$

where D_B is the elasticity bending matrix for an isotropic homogeneous material and B_B is the strain-displacement transformation matrix. This is more complicated than the membrane element and it is expressed in terms of the rotations of the normal of the initial surface. These are described quadratically over the surface as $\beta_j = \sum_{i=1}^{6} N_i \, \beta_{j,i}$ where $N_i = f(\xi, \eta)$ and ξ,η are the natural coordinates. Satisfying the Kirchhoff Hypothesis and relating the rotations to the normal displacement, β_j become: $\beta_j = \mathbf{H}_\mathrm{j}^\mathrm{T}(\xi, \eta)\mathbf{X}$, where X is the displacement matrix and $\mathbf{H}_\mathrm{x}^\mathrm{T}, \mathbf{H}_\mathrm{y}^\mathrm{T}$ are the new shape functions whose derivatives are used in the calculations and which are given explicitly in [12]. The strain displacement matrix is then

$$B_B\,(\xi, \eta) = \frac{1}{2A} \begin{bmatrix} y_{mi} \mathrm{H}_{x,\xi}^T + y_{ij} \mathrm{H}_{x,\eta}^T \\ -x_{mi} \mathrm{H}_{y,\xi}^T - x_{ij} \mathrm{H}_{y,\eta}^T \\ -x_{mi} \mathrm{H}_{x,\xi}^T - x_{ij} \mathrm{H}_{x,\eta}^T + y_{mi} \mathrm{H}_{y,\xi}^T + y_{ij} \mathrm{H}_{y,\eta}^T \end{bmatrix} \tag{12}$$

The integral of the bending stiffness matrix over the area A of the triangle is calculated using Gauss - Legendre Quadrature Integration as in Rathod [13].

When both matrices have been shaped, then for each discrete shell element the total stiffness matrix is assembled as $K_{STIFFe} = K_{CSTe} + K_{DKTe}$, and for the association of all shell elements and their nodes with their neighbours, a diagonal "supermatrix" is assembled which is filled with the stiffness matrices of each shell element K_{STIFFe}. To derive the total stiffness matrix, the "supermatrix" needs to be multiplied by the boolean matrix β and its transpose. The boolean matrix is created as in Davies [14] and contains the information regarding the connectivity of the elements.

$$K_{stiff} = \beta^T \cdot K_{STIFFe} \cdot \beta \tag{13}$$

Since the loading on the sail is already known as the result of the preceding aerodynamic calculation, then the system to be solved is of the form

$$K_{stiff} \cdot X = F \tag{14}$$

or

$$\begin{bmatrix} K_{STIFF1} & 0 & 0 \\ 0 & \ddots & 0 \\ 0 & 0 & K_{STIFFn} \end{bmatrix} \cdot \begin{Bmatrix} X_{1i} \\ \vdots \\ X_{ni} \end{Bmatrix} = \begin{Bmatrix} F_{1i} \\ \vdots \\ F_{ni} \end{Bmatrix} \tag{15}$$

where n is the node number and i is the i[th] degree of freedom. Some nodes are able to move while others are considered fixed. The latter carry a zero value of U_{ni}. Application of this boundary condition and prior to the solution of the system, enables the partitioning of the stiffness matrix and provides a matrix of smaller dimensions to solve, reducing thus the overall computation cost. The solution of the linear system is derived using LU decomposition.

2.3 Verification

As mentioned earlier, since the Lifting Surface formulation allows the treatment of the camber problem, only this allows the simulation of an asymmetrical airfoil by introducing her camber line as the surface chord. The NACA 4412 was chosen and modeled as a rectangular wing of 7.50 m span and 1.80 m chord (Figure 3) and the lattice was formed of 9 spanwise and 15 chordwise panels.

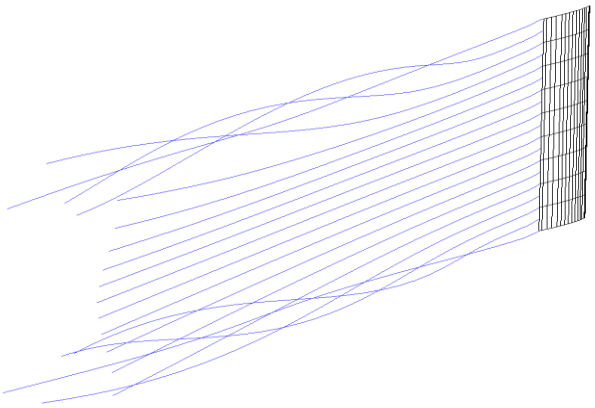

Figure 3. Cambered Wing Surface and Wake Roll-Up.

The surface was tested on three different Reynolds numbers 2×10^5, 5×10^5 and 10^6, corresponding to an inflow wind speed of about 3, 7 and 14 knots respectively.

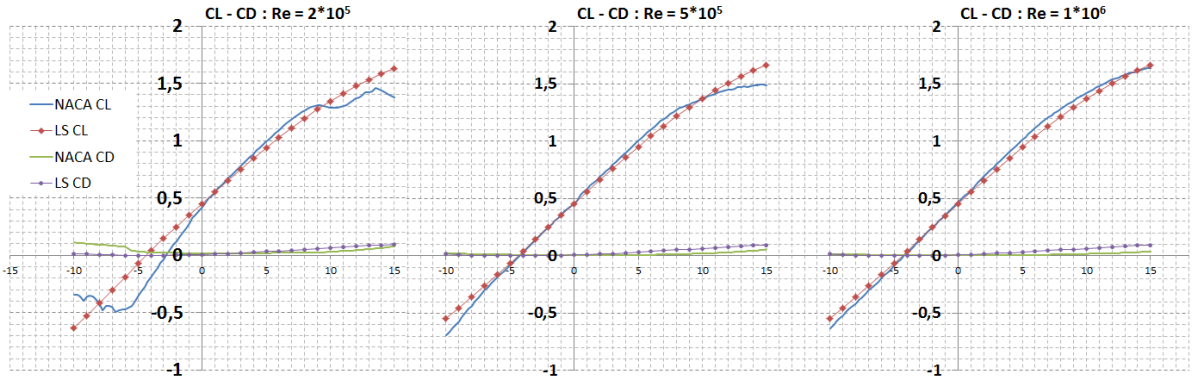

Figure 4. Lift and Drag Coefficients of Cambered Surface.

For smaller Reynolds numbers, as the angle of attack increases, separation occurs on a point that is relatively near the leading edge. Flow separation is not handled by L.S.T. which assumes the flow to be attached to the body. This explains the deviation of Lift Coefficients on the left part of Figure 4. As the inflow velocity increases the separation point moves backwards and L.S.T. seems more consistent with the real case. However viscous effects are always present and differences between the real case and computational results are unavoidable. Beyond the range of $(-10^o, 15^o)$ the error increased vastly and the calculated values cannot be taken into account. Lastly while the lattice was crude, in the aforementioned angle regime it approached the real values quite enough.

For the shell elements, a square 2 mm thick PET surface was subjected to a uniform pressure load of 20 kN/m^2, where the nodes around the perimeter were restrained from moving while the inner nodes were free and the same case was tested using commercial FEM package. In both cases the maximum deflection of the surface was 53 mm around the center of the surface. Points around the centre of the developed code carried a difference of less than a millimeter. However on the points around the perimeter the difference increased up to 3.5 mm (on the first inner perimeter). It is very probable that this is due to the way the boundary conditions are applied on each code. On Figure 5 the "z" displacements of both codes have been scaled by 10.

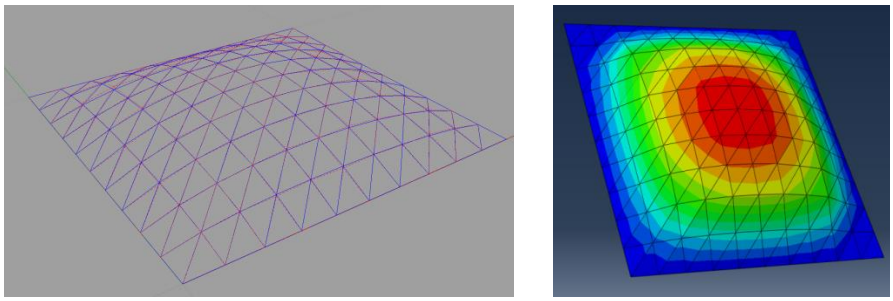

Figure 5. Bended under uniform pressure Surface using commercial FEM and shell elements.

3 CASE STUDY - RESULTS

The yacht under study is a 45' cruising hull whose hull geometry and loading conditions were available to the authors. The sails were modeled assuming an isotropic Kevlar surface. The yacht main dimensions and data are in table 1.

HULL	
Length Overall	13.90 m
Length Waterline	12.86 m
Beam Waterline	2.50 m
SAILS	
I (JIB)	15.70 m
J (JIB)	7.40 m
P (MAIN)	17.40 m
E (MAIN)	5.30 m
Young Modulus	1935 N/mm^2
Poisson Ratio	0.45
Thickness	0.8 mm

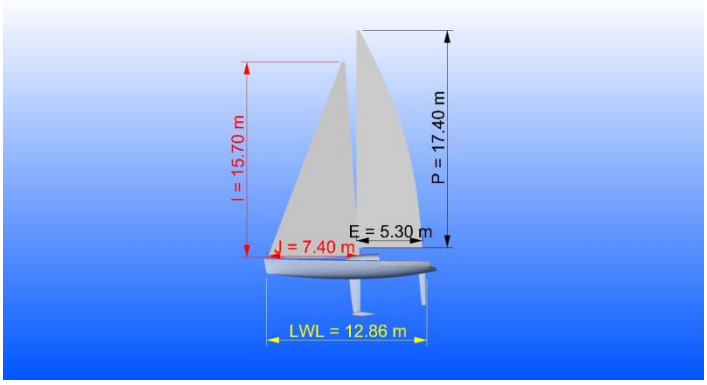

Table 1. Hull and Sails Dimensions and Material Data

The yacht was subjected to a set of wind speeds creating a series of C_L and C_D diagrams for the upwind sailing case, in the incoming flow angle of [0-40] degrees. As already mentioned in the verification part, the code overestimates the maximum C_L and transposes the stall angle further right than its real value, as separation effects are not handled by the current formulation. In the following graphs (Figure 6) are shown the C_L and C_D curves for relative wind speed of 10 knots. The number of necessary iterations for convergence is increasing in respect of the relative wind inflow angle, and reaches 25-30 iterations for very large angles. An example of converged shapes is appears in Figure 7.

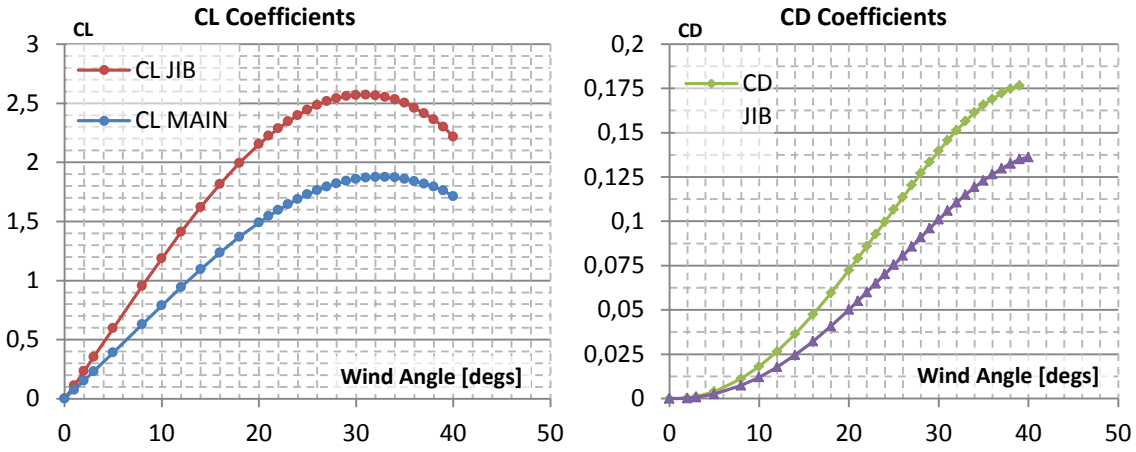

Figure 6. C_L-C_D diagrams, V_W= 10 kn.

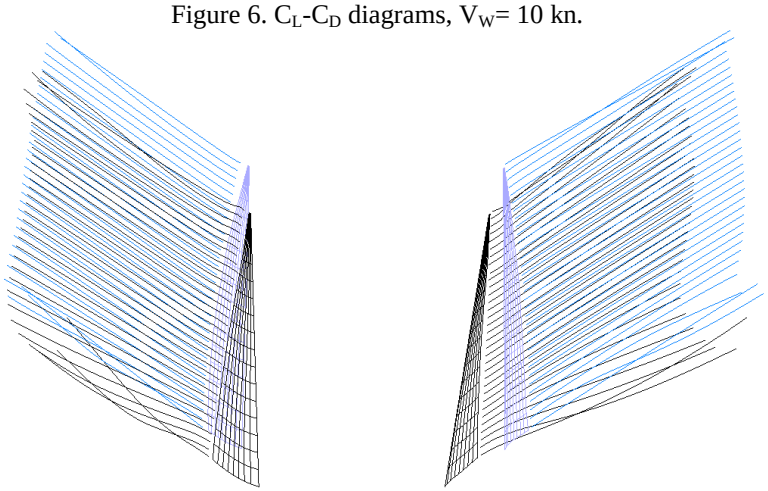

Figure 7. Two Sails System (Sails on flying shapes and Wake Streamlines)

4 CONCLUSIONS – FUTURE WORK

Two numerical schemes have been combined for the aerodynamic and structural modeling of sails under inflow wind. Both models balance the lack of detail with their computing speed allowing them to be implemented in an overall ship manoeuvring model. The Lifting Surface Vortex Lattice is a potential flow theory application that allows a thin object to be investigated by taking into account its camber line only. The triangular shell elements implemented in the finite element scheme can handle a deformation analysis of a thin isotropic surface under simple loading cases. The Lifting Surface method provides realistic results for a range of 20 to 25 degrees of fluid angle of attack around the leading edge, but as it doesn't take into account separation effects, it overestimates the lifting force of the sail and it increases the stall angle. The triangular shell element showed fair agreement with the results of a commercial package of FEM analysis for some simple tests. The model is crude, as sails were considered isotropic while they are usually orthotropic materials reinforced with fibers and wrinkling effects have been ignored.

Future work includes adding for the effects of a boundary layer, increase the order of the shell element in use, extend this model to a solver of unsteady cases and implementation of it into an overall model as a tool of investigating the directional instabilities of sailing yachts in waves.

5 ACKNOWLEDGEMENTS

The authors would like to thank Professor G. Politis of NTUA for his invaluable help. Also funding of Mr. Angelou's PhD Thesis by ELKE NTUA Research Fund is very deeply appreciated.

6 REFERENCES

[1] Ranzenbach, R., Xu, Z. (2005), "Sail Aero-Structures: Studying Primary Load Paths and Distortions" *The 17th Chesapeake Sailing Yacht Symposium,* Annapolis, Maryland, USA, March 2005.

[2] Graf, K., Renzsch, H. (2006), "RANSE Investigations of Downwind Sails and Integration into Sailing Yacht Design Processes", *2nd High Performance Yacht Design Conference,* Auckland, February 2006.

[3] Schoop, H., Besser, N., Taenzer, L. (1998), "On the Elastic Membrane in a Potential Flow", International Journal for Numerical Methods in Engineering, Vol. 41, pp. 271-291.

[4] Vernengo, G., Brizzolara, S. (2009), "Application of a Vortex Lattice Method to the Analysis of Sail Plans in Upwind Condition", *13th Congress of Intl. Maritime Assoc. of Mediterranean,* Istanbul, Turkey.

[5] Trimarchi D., Rizzo, C.M. (2009), "A FEM-MATLAB Code for Fluid-Structure Interaction coupling with application to sail aerodynamics of yachts", *13th Congress of Intl. Maritime Assoc. of Mediterranean,* Istanbul, Turkey.

[6] Falkner, V.M., (1943), "The Calculation of Aerodynamic Loading on Surfaces of Any Shape*"*, Reports and Memoranda No. 1910, London Great Britain.

[7] Spurk J.H, Aksel N., (2008), "*Fluid Mechanics*", Springer, Second Edition, Berlin, Germany.

[8] Katz J., Plotkin A., (2001), "*Low Speed Aerodynamics*", Cambridge University Press, Second Edition, Cambridge, UK.

[9] Willis C.J., Crapper G.D., Millward A., (1994), "A Numerical Study of the Hydrodynamic Forces Developed by a Marine Rudder" Journal of Ship Research Vol. 38, No. 3, Sept. 1994, pp. 182-192.

[10] Lee H., (2002), "Modeling of Unsteady Wake Alignment and Developed Tip Vortex Cavitation", PhD Thesis, University of Texas, Austin, Usa.

[11a] Zienkiewicz O.C., Taylor R.L., (2000), "*The Finite Element Method, Volume 1 : The Basis*", Butterworth – Heinemann, Fifth Edition, Oxford, UK.

[11b] Zienkiewicz O.C., Taylor R.L., (2000), "*The Finite Element Method, Volume 1 : Solid Mechanics*", Butterworth - Heinemann, Fifth Edition, Oxford, UK.

[12] Batoz J.L., Bathe K.J., Ho L.W., (1980), "A Study of Three-Node Triangular Plate Bending Elements". International Journal for Numerical Methods in Engineering, Vol. 15. 1771-1812.

[13] Rathod, H.T. et al, (2004), "Gauss Legendre Quadrature over a Triangle", J.Indian Inst. Sci.

[14] Davies A.J., (2011), "*The Finite element method : an introduction with partial differential equations*", Oxford University Press 2ND Edition, Oxford , UK.